Materials Today Bio 20 (2023) 100648

Contents lists available at ScienceDirect

Materials Today Bio

journal homepage: www.journals.elsevier.com/materials-today-bio

Facile and adhesive-free method for bonding nanofiber membrane onto thermoplastic polystyrene substrate to fabricate 3D cell culture platforms

Jaeseung Youn [a,1], Junyeol Rhyou [a,1], Dohui Kim [a], Jisang Lee [a], Jeong-Won Choi [b], Tae-Eun Park [b,**], Dong Sung Kim [a,c,d,*]

[a] Department of Mechanical Engineering, Pohang University of Science and Technology (POSTECH), 77 Cheongam-ro, Nam-gu, Pohang, Gyeongbuk, 37673, South Korea
[b] Department of Biomedical Engineering, College of Information and Biotechnology, Ulsan National Institute of Science and Technology (UNIST), Ulsan, 44919, South Korea
[c] Department of Chemical Engineering, Pohang University of Science and Technology (POSTECH), 77 Cheongam-ro, Nam-gu, Pohang, Gyeongbuk, 37673, South Korea
[d] Institute for Convergence Research and Education in Advanced Technology, Yonsei University, Seoul, 03722, South Korea

ARTICLE INFO

Keywords:
Nanofiber membrane
Thermal bonding
Polystyrene
3D cell culture
Microphysiological system

ABSTRACT

Nanofiber (NF) membranes have been highlighted as functional materials for biomedical applications owing to their high surface-to-volume ratios, high permeabilities, and extracellular matrix-like biomimetic structures. Because many *in vitro* platforms for biomedical applications are made of thermoplastic polymers (TP), a simple and leak-free method for bonding NF membranes onto TP platforms is essential. Here, we propose a facile but leak-free localized thermal bonding method for integrating 2D or 3D-structured NF membrane onto a TP supporting substrate while preserving the pristine nanofibrous structure of the membrane, based on localized preheating of the substrate. A methodology for determining the optimal preheating temperature was devised based on a numerical simulation model considering the melting temperature of the NF material and was experimentally validated by evaluating bonding stability and durability under cell culture conditions. The thermally-bonded interface between the NF membrane and TP substrate was maintained stably for 3 weeks allowing the successful construction of an intestinal barrier model. The applicability of the localized thermal bonding method was also demonstrated on various combinations of TP materials (e.g., polystyrene and polymethylmethacrylate) and geometries of the supporting substrate, including a culture insert and microfluidic chip. We expect the proposed localized thermal bonding method to contribute toward broadening and realizing the practical applications of functional NF membranes in various biomedical fields.

1. Introduction

In recent years, nanofiber (NF) membranes have been employed in various research and industrial fields, including biomedical engineering [1–4], air filtration [5], surface modification [6], electronics [7], and oil–water separation [8–10]. In particular, NF membranes have shown great potential in the development of *in vitro* organ/tissue models for drug testing or disease modeling, because they provide the structural or physical cues of *in vivo* tissue, such as extracellular matrix (ECM)- or basement membrane-like structures [11–15], high nutrient permeabilities [16,17], or stiffness at a physiological level [18]. In this regard, NF membranes have been utilized in the development of biomimetic *in vitro* cell culture platforms and have contributed to enhancing the physiological relevance of *in vitro* models for decades.

Abbreviations: BBB, blood–brain barrier; bFGF, basic fibroblast growth factor; BMEC, brain microvascular endothelial cells; BSA, bovine serum albumin; DAPI, 4′,6-diamidino-2-phenylindole; DMEM, Dulbecco's modified Eagle medium; DPBS, Dulbecco's phosphate-buffered saline; ECM, extracellular matrix; FBS, fetal bovine serum; FE-SEM, field-emission scanning electron microscope; GFAP, glial fibrillary acidic protein; iPSC, induced pluripotent stem cell; NF, nanofiber; PBS, phosphate buffer saline; PCL, polycaprolactone; PMMA, polymethylmethacrylate; PS, polystyrene; RT, room temperature; SEM, scanning electron microscope; SFM, serum free medium; TEER, transepithelial electrical resistance; TP, thermoplastic polymers; UM, unconditioned medium.

* Corresponding author. Department of Mechanical Engineering, Pohang University of Science and Technology (POSTECH), 77 Cheongam-ro, Nam-gu, Pohang, Gyeongbuk, 37673, South Korea.
** Corresponding author.
E-mail addresses: tepark@unist.ac.kr (T.-E. Park), smkds@postech.ac.kr (D.S. Kim).
[1] These authors contributed to this work equally.

https://doi.org/10.1016/j.mtbio.2023.100648
Received 28 February 2023; Received in revised form 19 April 2023; Accepted 27 April 2023
Available online 29 April 2023

To utilize NF membranes in the development of biomimetic cell culture platforms for physiological *in vitro* models, NF membranes should be integrated with a culture substrate, which can range in variety from a conventional Petri dish and culture insert to a microfluidic chip. The culture substrates are usually made of thermoplastic polymers (TP) such as polystyrene (PS) or polymethylmethacrylate (PMMA). It is especially important that the bonding interface between the TP substrate and NF membrane (TP–NF bonding interface) be formed such that delamination of the NF membrane and leakage are substantially prevented [19]. However, unlike typical flat membranes, the integration of NF membranes on TP substrates has been found to be challenging owing to the unique characteristics of NF membranes, especially for biological applications. Specifically, the roughness of the NF membrane surface hinders the formation of conformal contact, which is crucial for creating strong bonding interfaces, on TP substrates [20,21]. Moreover, because the pores between the nanofibers frequently result in the filtration of liquids, the use of a liquid chemical adhesive for NF membrane integration is also limited because the liquid adhesive can damage the NF membrane near the bonding region (Fig. S1).

Therefore, despite the widespread use of NF membranes, the integration of NF membranes onto TP substrates is typically accomplished through less than ideal means, including with solid adhesives such as double-sided adhesive tapes [22–24]; clamping systems with bolts and nuts; or interference fits, which usually require complex and elaborate handling [25–27]. Unfortunately, a solid adhesive on an NF membrane can lose its bonding strength in humid environments, and the adhesion material may affect cell viability and function. Furthermore, clamping systems and interference fitting typically require complex and multiple manual integration processes, which distort the NF membrane at the integration region. However, owing to the lack of an appropriate method for bonding NF membranes onto TP cell culture substrates, most NF membrane-based culture platforms, even in commercial products, rely on the aforementioned bonding methods, which have their own limitations. Therefore, the development of a simple but leak-free bonding method that does not rely on an external material or device is definitely valuable for the stable fabrication of NF membrane-based *in vitro* culture platforms and their extensive use.

Herein, we propose a facile, leak-free, and structural-damage-free method for bonding an NF membrane onto a TP substrate via localized heating. We present a numerical simulation model for the optimization of the preheating temperature for successful bonding, which successfully predicts the heat-transfer phenomena during thermal bonding. Appropriate localized thermal bonding conditions were obtained numerically and experimentally according to the various material properties of the NF membrane and TP substrate. At the proper conditions, only the NFs on the locally preheated region of the TP substrate were selectively melted, thereby forming a TP–NF bonding interface. The localized thermal bonding method was found to be not only sufficiently strong to be comparable with conventional bonding methods using solid adhesives, but also leakage-free and long-lasting. We demonstrated the practical applicability of the proposed localized thermal bonding method by culturing human intestinal Caco-2 epithelial cells on a polycaprolactone (PCL) NF membrane, which was thermally bonded onto a PS culture insert for 21 days in a stable manner. The localized thermal bonding method enables the integration of 2D or even 3D NF membranes on a TP substrate with various and complex geometries (e.g., culture insert, chamber, plate, microfluidic chips), allowing the fabrication of many types of NF membrane-integrated culture platforms for dynamic culture models, coculture models, and even 3D spheroid culture models.

2. Materials and method

2.1. Fabrication of thermoplastic supporting substrates

A 24-well PS culture insert with no membrane at the bottom end was custom-designed and produced using PS pellets (DowChem, USA) and an injection molding machine (SE50D; Sumitomo, Japan). The injection-molded PS culture inserts were washed using a commercial detergent (LG, South Korea) and 70% ethanol (Samchun Chemical, South Korea) to remove the remaining materials and oils from the inserts before bonding. Before the injection molding process, the PS pellets were completely dried in a 70 °C oven. The metal mold was designed and custom-made (Shinil Precision, South Korea) to have two cavities for molding the PS pellets into the shape of the designed insert. The injection molded inserts were compatible with the commercial 24-well plate (Corning, USA). The microfluidic chip and culture chamber were fabricated from a polymethylmethacrylate (PMMA) plate (Acriyl Choi-ga, South Korea) using a laser-cutting machine (MachineShop, South Korea).

2.2. Nanofiber membrane fabrication

PCL (Mn = 80,000 g mol^{-1}) (Sigma Aldrich, USA) pellets were dissolved in a mixture of methanol (Sigma Aldrich, USA) and chloroform (Sigma Aldrich, USA) (1:3; v/v) at a concentration of 7.5 wt%, in accordance with previous studies [24,28]. The PCL solution was mounted on a 5-mL gastight glass syringe (Hamilton, USA), and a metal needle (23G) was connected for electrospinning. An electrospinning machine (ESR200R2; NanoNC, South Korea) was used in conjunction with a ring collector of diameter 2 cm at an applied voltage of 18 kV. The distance between the needle and ring collector was set to 10 cm, and the flow rate of the PCL solution was set to 1 mL h^{-1}. Electrospinning was performed for 10 min, resulting in a free-standing PCL NF membrane on the ring collector. To prepare a PCL/Pluronic F-108 (PCL-F) NF membrane, a mixture of PCL (Mn = 80,000 g mol^{-1}) and Pluronic F-108 (Sigma Aldrich, USA) (1:1; w/w) was dissolved in 1,1,1,3,3,3-hexafluoro-2-propanol (Sigma Aldrich, USA) at a concentration of 5 wt%. Electrospinning was conducted using a ring collector with a diameter of 2 cm at an applied voltage of 17 kV. The distance between the needle and ring collector was set to 20 cm, and the flow rate of the PCL solution was set to 1 mL h^{-1}. A 3D nanofiber microwell was fabricated using a matched-mold embossing device, based on a procedure developed in a previous study [16]. The mold was developed using polydimethylsiloxane (10:1 curing ratio) and had the geometry to create an NF microwell with a depth and diameter of 600 μm.

2.3. Thermal bonding of NF membrane

The bonding surface at the bottom end of the PS insert was locally heated for 10 min at desired preheating temperature using a commercial hot plate (Corning, USA). The locally heated PS culture insert was transferred to the prepared free-standing NF membrane or NF microwell without applying extra pressure. For the control group, solid adhesive (467 MP; 3 M, USA) was cut by using a laser cutting machine and used to bond the NF membranes on the PS insert.

2.4. Calculation of undamaged area after thermal bonding

The undamaged area of the nanofiber membrane after thermal bonding was calculated using the following equation:

$$\textit{Undamaged area}(\%) = \frac{\textit{Measured area of the undamaged nanofiber memebrane}}{\textit{Area of the total circular nanofiber membrane}} \times 100$$

The undamaged nanofiber membrane was measured based on the area of the white region, which was determined using the ImageJ software. The area of the entire circular nanofiber membrane was 16 mm^2.

2.5. Heat transfer simulation

The temperature distribution induced by the heat transfer from the PS culture insert to the PCL NF membrane was numerically evaluated using the COMSOL Multiphysics v5.0 (COMSOL, USA) software. As a representative case for their respective geometries, the PS culture insert and PCL NF membrane were used as the TP substrate and NF membrane, respectively. A 2D heat transfer simulation model with a time-variant condition was used to examine the temperature distribution of the axisymmetric geometry of the culture insert and NF membrane during the bonding process. The PCL NF membrane was employed as a thin membrane with a thickness of 30 μm and placed on the wall of the PS culture insert, which had a thickness of 1 mm. The distance between the wall of the PS culture insert and the central axis was set to 4 mm, following an actual PS culture insert. Although the average diameter of the PCL NF was approximately 700 nm, the thermal conductivity of the PCL NF was set two-fold that of the bulk material [29,30]. The porosity of the PCL NF membrane was calculated to be approximately 79.5% using the following equations [31]:

$$Apparent\ density\left(g\ cm^{-3}\right) = \frac{mass\ of\ membrane\ (g)}{membrane\ thickness\ (cm) \times membrane\ area\ cm^2},$$

$$Porosity\ (\%) = \left(1 - \frac{apparent\ density\ (g\ cm^{-3})}{bulk\ density\ (g\ cm^{-3})}\right) \times 100\%$$

Finally, the effective thermal conductivity of the PCL NF membranes was calculated using the following equation:

$$k_{eff} = \left[\frac{\varepsilon}{k_f} + \frac{(1-\varepsilon)}{k_s}\right]^{-1}.$$

(ε: porosity, K_S: NF thermal conductivity, and K_f: air thermal conductivity).

The effective thermal conductivity of the PCL NF membrane was calculated to be approximately 0.022 W m^{-1} K^{-1}. The material properties of the PS culture inserts were determined based on the datasheet provided by the supplier. The boundary condition for external natural heat convection was applied to the PS wall, which did not come in contact with the PCL NF membrane. A boundary condition for thermal contact was applied to the bonding interface. Various initial temperatures for the PS culture insert were set, and the corresponding spatio-temporal changes in the temperature variation due to heat transfer were obtained. Contour lines were drawn to show the boundary temperatures and distinguish the regions where melting began.

2.6. Scanning electron microscope (SEM) imaging

Structural changes in the PCL NF membrane after thermal bonding were examined using a field-emission scanning electron microscope (FE-SEM) (SU6600; Hitachi, Japan). The NF membrane-bonded PS culture insert (referred to hereafter as an NF insert) was sputter-coated with platinum at a current of 20 mA for 120 s. The structures of both the NFs at the TP–NF bonding interface and at the free-standing region were captured and examined.

2.7. Indentation test

The bonding strength between the NF membrane and PS insert was evaluated via an indentation test. The indentation force was measured using a custom-designed indentation machine composed of a linear stage, load cell, and force indicator [11]. The indentation speed was set to 0.1 mm s^{-1}. The diameter of the indenter head was 2 mm. The nanofiber membrane specimen had a diameter of 8 mm and a thickness of 30 μm. Both the indentation force and displacement of the indenter were measured in real time and saved in an Excel file format. The maximum indentation force was observed immediately before the NF membrane was penetrated, after which this force decreased dramatically.

2.8. Cell culture

The fabricated NF insert was plasma treated using an air plasma machine (VITA1; Femto Science, South Korea) to render it hydrophilic. The PCL NF membrane was then coated via incubation with an ECM solution composed of type I collagen (Corning, USA) and Matrigel (Corning, USA) mixed in phosphate buffer saline (PBS) at a concentration of 0.15 mg mL^{-1} for 1 h at 37 °C (Fig. S2). Human intestinal Caco-2 epithelial cells (Korean Cell Line Bank, South Korea) were seeded in each NF insert at a cell density of 3×10^5 cells mL^{-1} and cultured with Dulbecco's modified Eagle medium (DMEM; Gibco, USA) supplemented with 10% (v/v) of fetal bovine serum (Gibco, South Korea), 1% (v/v) penicillin/streptomycin solution (Gibco, USA), and 1% (v/v) amphotericin B (Gibco, USA). The Caco-2 cells were cultured for 21 days in a humidified CO_2 incubator at 37 °C with 5% CO_2, and the culture medium was replaced every two days.

HaCaT and NIH3T3 cells were cultured in DMEM supplemented with 10% (v/v) fetal bovine serum (FBS) and 1% (v/v) amphotericin B. Type I collagen hydrogel solution was prepared by mixing type I collagen solution, 1 M NaOH (Sigma-Aldrich, USA), and 10x DMEM (Gibco, USA) at a volume ratio of 1 : 0.025: 0.1. NIH3T3 cells were mixed with the prepared type I collagen hydrogel solution at a density of 1×10^6 cells mL^{-1}, and the cell-laden hydrogel solution was introduced to the area below the NF membrane of the NF microfluidic chip. After gelation of the collagen hydrogel at 37 °C for 1 h, HaCaT cells were seeded onto the NF membrane at a density of 5×10^6 cells mL^{-1}. The HaCaT cells and NIH3T3 cells were cultured for 3 days under the top channel flow at a rate of 60 μL h^{-1} in a humidified CO_2 incubator at 37 °C with 5% CO_2.

A human induced pluripotent stem cell (iPSC) line (IMR90-4; WiCell Research Institute, USA) was purchased and maintained on Matrigel (Corning, USA) using TeSR™-E8™ (Stemcell Technologies, Canada). The cells were cultured according to the WiCell Feeder Independent Pluripotent Stem Cell Protocols provided by the WiCell Research Institute (http://www.wicell.org). The human iPSCs were differentiated into brain microvascular endothelial cells (iPSC-BMECs) with minor modifications [18]. The differentiation process was as follows: The iPSCs were singularized using Accutase (Merck, USA) and seeded on a Matrigel-coated 6-well plate at a density of 1.7×10^4 cells per well in TeSR™-E8™ supplemented with 10 μM ROCK inhibitor (Y-27632; Tocris Bioscience, UK) on D-3. The iPSCs were then cultured for another two days without the ROCK inhibitor until the cell density reached 2.5×10^5 cells per well. On D0, the medium was switched to a differentiation medium (unconditioned medium; UM). The UM was composed of 78.5 ml DMEM/F12 (Thermo Fisher Scientific, USA), 20 mL Knockout™ Serum Replacement (Thermo Fisher Scientific, USA), 1 mL Non-Essential Amino Acids (100 ×) (Thermo Fisher Scientific, USA), 0.5 mL GlutaMAX™ supplement (Thermo Fisher Scientific), and 182 μl β-mercaptoethanol (Thermo Fisher Scientific, USA). After a day, the culture medium was changed every day for another five days. Next, to selectively expand the endothelial cells, the medium was changed to EC + RA medium, which is a Human Endothelial Serum Free Medium (SFM) (Thermo Fisher Scientific, USA) supplemented with 1% human serum (Sigma-Aldrich, USA), 20 ng mL^{-1} human basic fibroblast growth factor (bFGF; PeproTech, USA), and 10 μM retinoic acid (Sigma-Aldrich, USA). On D8, the differentiated cells were detached, singularized with Accutase, and seeded onto the NF inserts to simulate the blood–brain barrier (BBB). To improve the BBB attributes of the iPSC-BMECs, the cells were exposed to low oxygen tension (5% O_2, 5% CO_2) during differentiation from D0 to D9 using a hypoxic chamber (Galaxy® 48 R; Eppendorf), in accordance with a previous study [18]. Human primary astrocytes (Cat#1800; ScienCell, USA) were

purchased and maintained in T75 flasks containing Astrocyte Medium (ScienCell, USA). The astrocytes were detached one day before the seeding of the iPSC-BMECs. The astrocytes were seeded on the bottom of the insert at a density of 0.1×10^4 cells per insert and incubated for 1 h to attach onto the coated membrane. The insert was then flipped and incubated in the 24-well plate for a day.

The WTC-11 iPSC cell line (Coriell Institute for Medical Research, GM25256) was cultured in feeder-free conditions on 6-well culture plates coated with 1% GelTrex (Thermo Fisher Scientific, A1413302) using mTeSRTM1 (Stem Cell Technologies, 85850) in a 37 °C incubator with 5% CO_2. The iPSCs were passaged according to the manufacturer's protocol every 4 days using ReLeSRTM (Stem Cell Technologies, 05872). For the formation of iPSC spheroid in 3D NF microwell bonded on the culure insert, the sterilized NF microwell were coated with 0.025% agarose (Thermo Fisher Scientific, A4018) for 3 h to prevent cell attachement on the bottom of NF microwell. The dissociated iPSCs were seeded into NF microwell arrays at an average density of 10,000 per individual microwell using mTeSRTM1 and cultured for 24 h in a 37 °C incubator with 5% CO_2.

2.9. TEER measurement and immunofluorescence imaging

The transepithelial electrical resistance (TEER) of the Caco-2 epithelium cultured on the ECM-coated PCL NF membrane was measured using a TEER measurement equipment (EVOM2; World Precision Instruments, USA). The TEER value of the Caco-2 epithelium was calculated via subtraction of the TEER value of the membrane without cells, in accordance with a previous study [32].

For immunofluorescence imaging of the Caco-2 cells after 21 days of culture, the cells were prepared using the following procedures: (1) fixation with 4% (w/v) paraformaldehyde for 15 min at room temperature (RT); (2) permeabilization of the cell membrane with 0.3% (v/v) Triton X-100 solution for 30 min at RT; and (3) treatment with blocking solution (1% w/v bovine serum albumin (BSA)) for 1 h at RT. The cells were washed with PBS between steps. The cells were then incubated with a primary antibody solution of ZO-1 (61–7300; Invitrogen, USA) or P-gp (MA5-13854; Invitrogen, USA) diluted in PBS at a concentration of 1% (v/v) for 12 h at 4 °C. After the cells were washed with PBS 5 times, they were incubated with a secondary antibody solution of Alexa Fluor 488 or 568 (A-11011 or A-10680; Invitrogen) diluted in PBS at a concentration of 0.5% (v/v) for 3 h at RT. After PBS washing 3 times, 4,6-diamidino-2-phenylindole dihydrochloride (DAPI; Thermo Fisher, USA) and Alexa Fluor phalloidin 680 (A22286; Invitrogen, USA) diluted in PBS at a concentration of 0.5% (v/v) were added at RT for 1 h to visualize the cell nuclei and F-actin, respectively. The immunofluorescence-stained cells were imaged and examined using a confocal microscope (FV3000; Olympus, Japan) and the Imaris software (Oxford Instruments, UK). The HaCaT and NIH3T3 cells in the NF microfluidic chip were fixed using the same process as that used for the Caco-2 cells and stained with phalloidin and DAPI. The iPSC spheroids were stained using a live/dead assay kit (Invitrogen, USA), in accordance with the product manual. The stained iPSC spheroids, HaCaT, and NIH3T3 cells were also imaged using the same FV3000 confocal microscope and examined using the Imaris software.

The iPSC-BMECs and astrocytes were fixed with 4% paraformaldehyde (Biosesang, South Korea) for 15 min and permeabilized with 0.1% Triton-X100 (Sigma-Aldrich, USA) in Dulbecco's phosphate-buffered saline (DPBS) for 10 min at RT. Next, the samples were blocked with 10% goat serum in 0.1% Triton-X100 for 1 h at RT, and then, an adequate concentration of the primary antibodies in 10% goat serum (Thermo Fisher Scientific, USA) in DPBS were treated overnight at 4 °C. Primary antibodies of ZO-1 (Invitrogen, USA) and glial fibrillary acidic protein (GFAP) (Novus, USA) were used to stain the iPSC-BMECs and astrocytes, respectively. After the samples were washed with DPBS three times, the fluorescent dye-conjugated secondary antibodies were incubated for 1 h at RT. Nuclei and F-actin were counterstained with 1 μg mL^{-1} of DAPI (Sigma-Aldrich, USA) and 1:400 dilution of phalloidin (Invitrogen, USA). After washing, a mounting medium (Leica, Germany) was added to both cells and the bottom of the insert for integration with the cover glass for imaging. Fluorescent images of the cells were obtained using a confocal microscope (LSM980; Zeiss, Germany).

3. Results

3.1. Localized thermal bonding of NF membrane on TP substrate

We propose a localized thermal bonding method for integrating 2D or 3D NF membranes on TP substrates, allowing the fabrication of various types of NF membrane-integrated cell culture platforms without the use of any external adhesive or bonding device, as shown in Fig. 1a. The concept of the proposed localized thermal bonding method is shown in Fig. 1b. The bonding surface of the TP substrate was locally heated to a temperature that was determined over the melting temperature of the prepared NF. When the free-standing NF membrane was brought to the TP substrate, only the NFs that touched the preheated bonding surface of the TP substrate were selectively melted and bonded owing to heat transfer, forming a TP–NF bonding interface. At the same time, the NFs in the free-standing region, which did not have physical contact with the bonding surface, maintained their pristine nanofibrous structure. As proof of concept, we applied the thermal bonding method to the integration of a PCL NF membrane, which is a highly biocompatible and widely used material in biomedical applications, on a PS thermoplastic culture substrate. The PCL NF membrane had a thickness of 30 μm, fiber diameter of 689 ± 22 nm, and pore size below 4 μm (Fig. S3). Fig. 1c shows the SEM images of the PCL NF membrane bonded onto the PS substrate via localized thermal bonding. The images show the region-specific structures of the PCL NF membrane between the bonding interface and the free-standing region. The NFs in the free-standing region maintained their intact nanofibrous structure, whereas the NFs on the TP–NF bonding interface melted and bonded onto the PS substrate after losing their original nanofibrous structure. The boundary dividing the free-standing region and TP–NF bonding interface can be clearly distinguished by its structure. These results indicate that the NF membrane can be successfully integrated with a TP substrate while maintaining its original nanofibrous structure in a free-standing manner, using the localized thermal bonding method.

3.2. Heat transfer simulation of localized thermal bonding

Although polymeric materials for NFs such as PCL are typically vulnerable to heat, their unique nanofibrous structures must be well maintained after the localized thermal bonding process. In this regard, the localized thermal bonding process for NF membranes should be carefully tuned to provide sufficient heat to selectively melt the NFs at the TP–NF bonding interface without affecting NFs in the free-standing region. Therefore, we attempted to optimize the preheating temperature of the TP substrate to achieve selective and localized melting of NFs via numerical simulations of heat transfer from the TP substrate to the NF membrane.

Using the COMSOL software, we numerically simulated the spatio-temporal temperature distribution induced by heat transfer near the TP–NF bonding interface for the NF membrane on the preheated PS (Fig. 2a (i)–(ii)). As a representative case, the material properties and geometries of the PCL NF membrane and commercial TP substrate (24-well PS culture insert) were referred to in the simulation model. The temporal temperature variation results of the simulation were compared with experimental data from actual temperature measurements at the bonding interface of the bottom end of the preheated PS culture insert, monitored using a thermal imaging camera (FLIR E40; Teledyne FLIR, USA) (Fig. 2a (iii)). The temporal decrease in temperature due to heat

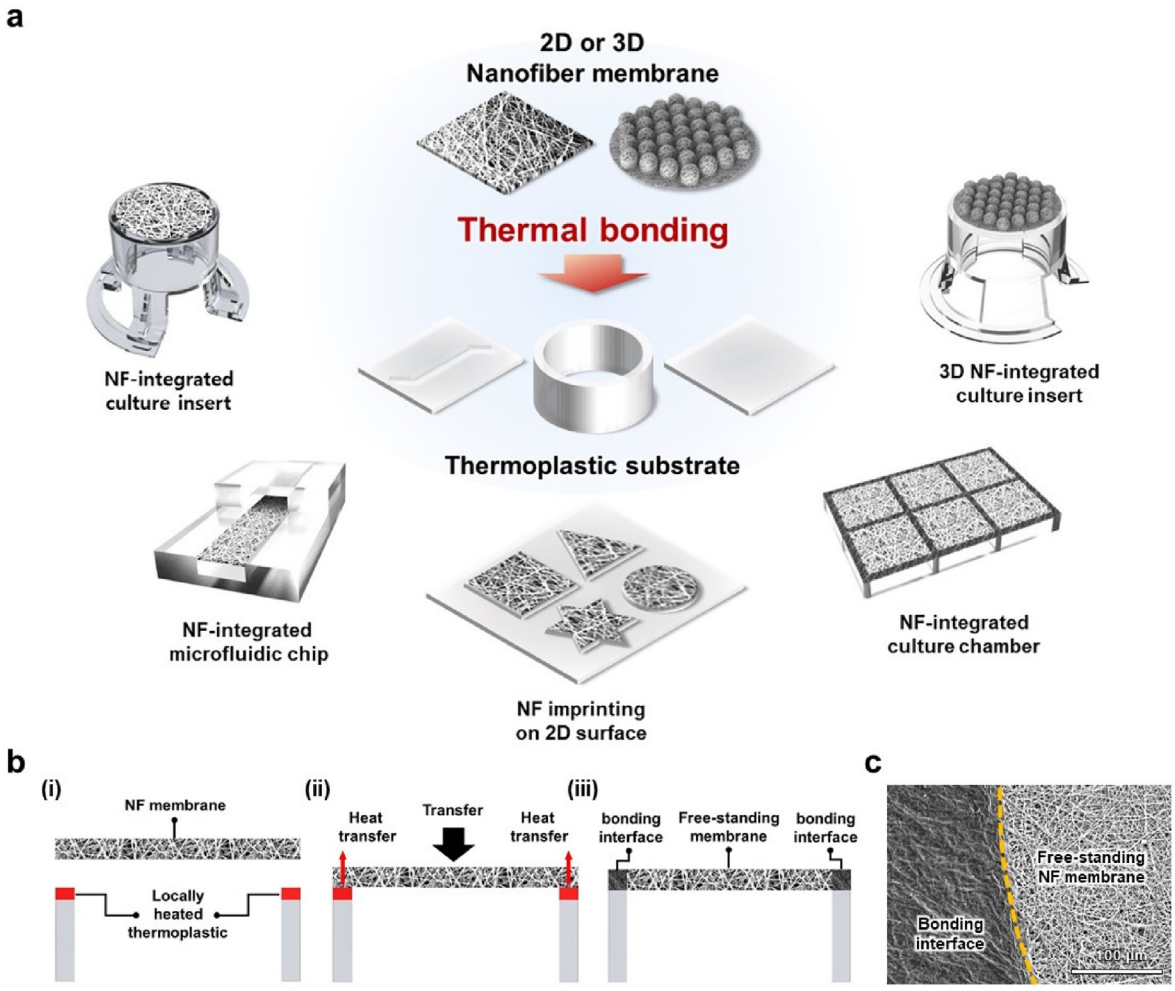

Fig. 1. (a) Schematic illustration demonstrating applicability of proposed thermal bonding method for fabrication of 2D or 3D NF-membrane integrated culture platforms. (b) Concept of proposed localized thermal bonding method. (c) SEM image of TP–NF bonding interface, showing clear boundary between bonding interface and free-standing area.

transfer derived from the numerical results was very similar to the actual temperature change at the bonding interface of the bottom end of the PS culture insert, validating the proposed simulation model (Fig. 2a (iv)).

We determined the preheating temperature of the PS culture insert, denoted by T_{PS}, applied to the localized thermal bonding of the PCL NF membrane based on the heat transfer simulation results. T_{PS} was set starting from 55 °C, which is near below the melting temperature of the PCL ($T_{m\text{-}PCL}$; ~60 °C), and was increased gradually to 75 °C at 5 °C intervals. We conducted heat transfer simulations and obtained temperature distributions near both the TP–NF bonding interface and free-standing regions. Temporal changes in the maximum temperature of the NF membrane, denoted by T_{NF}, in the free-standing region ($T_{NF\text{-}FS}$) and TP–NF bonding interface ($T_{NF\text{-}BI}$) at each condition are shown in Fig. 2b. The temporal change in $T_{NF\text{-}FS}$, where the nanofibrous structure should be maintained, was plotted for each condition (Fig. 2b(iv)), showing that $T_{NF\text{-}FS}$ only slightly increased during the first 1 s and decreased in slow manner due to the heat transfer from the pre-heated PS insert. From the simulation results, both $T_{NF\text{-}FS}$ and $T_{NF\text{-}BI}$ at each condition were obtained and plotted in Fig. 2c (i). When T_{PS} was 60 °C, which is near $T_{m\text{-}PCL}$, $T_{NF\text{-}BI}$ could not reach $T_{m\text{-}PCL}$, preventing localized thermal bonding from proceeding successfully and completely. By contrast, when T_{PS} was over 70 °C, which is far above $T_{m\text{-}PCL}$, $T_{NF\text{-}FS}$ also went over $T_{m\text{-}PCL}$, which could result in the structural damage of NFs in the free-standing region. When T_{PS} was set to 65 °C, $T_{NF\text{-}BI}$ went over $T_{m\text{-}PCL}$, while $T_{NF\text{-}FS}$ was maintained below $T_{m\text{-}PCL}$.

We performed localized thermal bonding experiments for various T_{PS} values and compared the data with the simulation results. The SEM images of the NFs at the TP–NF bonding interface and free-standing region show clear differences depending on T_{PS} (Fig. 2c (ii)). As expected from the simulation results, when T_{PS} was 55 °C, the NFs at the TP–NF bonding interface were not fully melted, thereby failing to produce reliable bonding between the PCL NF membrane and PS culture insert. By contrast, when T_{PS} was 75 °C, melting of the PCL NFs and damage to the nanofibrous structure occurred not only at the TP–NF bonding interface but also in the free-standing region. At the optimal condition of T_{PS} ~65 °C for localized thermal bonding, which was proposed based on the simulation, the PCL NFs melted and bonded onto the PS substrate only at the TP–NF bonding interface.

These microscopic structural behaviors can also be observed on a macroscopic scale. When the PCL NFs melted and lost their nanofibrous structure, the original white PCL NF membrane became transparent. When T_{PS} was 55 °C, the PCL NF membrane on the PS substrate showed no transparent region even at the TP–NF bonding interface (indicated by a black arrow in Fig. 2d (i)) after the bonding process. By contrast, the PCL NF membrane bonded at the optimal T_{PS} (65 °C) showed a transparent region only at the TP–NF bonding interface (indicated by the red arrow in Fig. 2d (ii)). Lastly, as expected, a T_{PS} of 75 °C caused damage to the NFs at the free-standing region; the NFs lost their original nanofibrous structures, and transparent parts were observed even in the free-standing region (indicated by a red arrow in Fig. 2d (iii)). The portion of

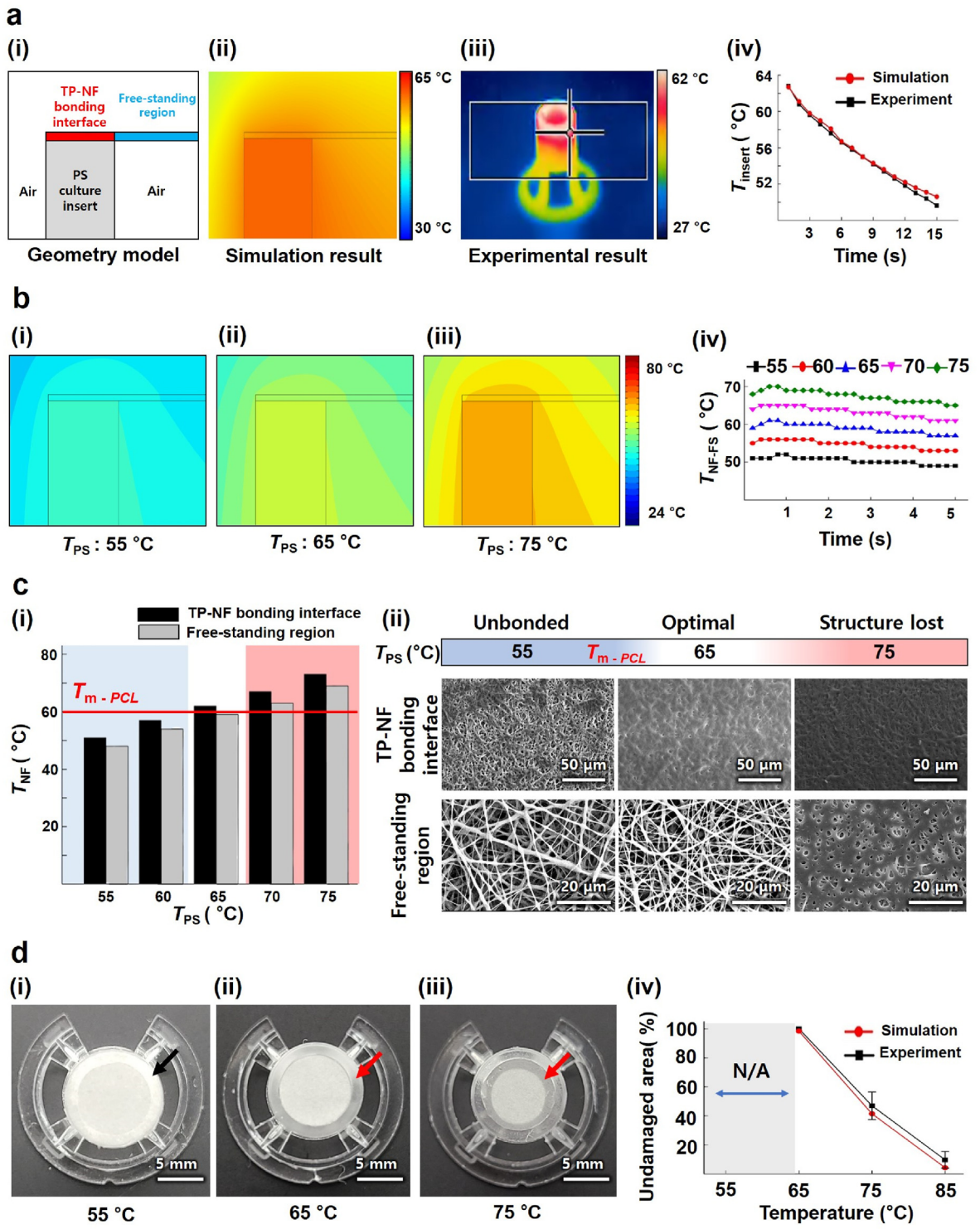

Fig. 2. (a) Setup of simulation model and comparison with experimental result: (i) geometry model used for heat transfer simulation, (ii) simulation result obtained from previous model, (iii) thermal camera image during actual heat loss of locally heated PS culture insert, and (iv) comparison of heat loss of PS culture insert between simulation and experimental results. (b) Temperature distribution of NF membrane: (i) contour line of temperature when T_{PS} was set to 55 °C, (ii) 65 °C, (iii) 75 °C, and (iv) $T_{NF\text{-}FS}$ depending on T_{PS}. (c) Optimization process for preheating temperature: (i) temperature difference between TP–NF bonding interface and free-standing region, where the red line indicates $T_{m\text{-}PCL}$, (ii) SEM image of TP–NF bonding interface and free-standing region. Optimal T_{PS} is shown in the white section. (d) Structurally damaged area depending on the preheating temperature: (i) image of NF insert, insert_th, when T_{PS} was 55 °C, (ii) 65 °C, and (iii) 75 °C, and (iv) comparison of undamaged area between simulation and experiment. (For interpretation of the references to color in this figure legend, the reader is referred to the Web version of this article.)

the undamaged nanofibrous region, where the free-standing NFs maintained their original structures after bonding, could also be successfully estimated based on our simulation model (Fig. 2d (iv)).

3.3. Mechanical evaluation of bonding strength

To mechanically evaluate the bonding strength between the NF membrane and PS substrate, an indentation test was performed using a customized indentation machine [23]. A schematic of the indentation test is shown in Fig. 3a (i). The NF insert prepared via localized thermal bonding (denoted by NF insert_th) was placed on a base substrate. A linear stage controller and force indicator were connected to a computer, and the linear stage was controlled using a customized control panel. Using the linear stage, the indenter pushed the center of the NF membrane until the NF membrane was ruptured and fully penetrated by the indenter. For this experiment, we prepared NF inserts composed of a PCL NF membrane and PS culture insert as a representative case. For comparison, we also prepared samples bonded using a conventional solid adhesive (denoted by NF insert_ad).

Force–displacement curves obtained from the indentation tests show that the force increment behaviors with respect to the indentation displacements of the NF membranes of the various NF insert_th samples are comparable to those of the NF insert_ad samples, although the NF membranes bonded at 75 °C show further increments of the indentation force due to changes in the material properties of the NFs (Fig. 3a (ii)). Finally, the evaluation results for the maximum indentation force of each NF membrane in Fig. 3a (iii) show that the maximum indentation force of NF insert_th bonded at 65 °C is similar to that of NF insert_ad; by comparison, a lower maximum indentation force was measured for 55 °C (below $T_{m\text{-}PCL}$), and a greater maximum indentation force was measured for 75 °C (highly over $T_{m\text{-}PCL}$).

We further examined the bonding stabilities of NF insert_ad and NF insert_th at wet conditions by exposing them to cell culture media for 3 days (Fig. 3b). In the case of NF insert_ad (Fig. 3b (i)), the NF membrane was stably bonded and showed no delamination. However, in the case of the NF membrane of the NF insert_th sample bonded at 55 °C (Fig. 3b (ii)), the NFs did not melt on the TP–NF bonding interface, failed to bond properly onto the PS culture insert, and thus were delaminated. By contrast, the NF membrane of the NF insert_th sample bonded at 65 °C (Fig. 3b (iii)) was stably bonded like in a solid adhesive bond.

3.4. Bonding stability under cell culture conditions

We cultured the cells on both the NF insert_ad and NF insert_th samples to further examine whether bonding between the NFs and TP was sufficiently robust to maintain a tight sealing under cell culture conditions for long culture times. We selected the human intestinal Caco-2 cell line because the cell line is known to form a monolayer on the membrane. A Caco-2 monolayer and an underlying NF membrane form a physical barrier that separates the space above and below the cell monolayer–NF membrane.

Immunofluorescence images in Fig. 4a show the cellular structures and differentiation markers of Caco-2 cells, including a tight junction protein Zo-1 (ii) and an efflux protein P-gp, (iii) cultured for 21 days in NF insert_th at 65 °C. The results demonstrated that the thermally bonded NF membrane could stably support the Caco-2 cells for 21 days until they were differentiated. We also measured the TEER value to determine whether the Caco-2 monolayer and underlying NF membrane formed a tight barrier dividing the inside and outside of the PS culture insert without delamination at the TP–NF bonding interface (Fig. 4b (i)). Notably, the TEER value of the Caco-2 monolayer in NF insert_th increased over time, indicating that the NF membrane was well-bonded onto the PS culture insert without any gaps. The NF insert_ad sample exhibited a similar TEER value to that of NF insert_th only for the first few days, whereas the increment in the TEER value was significantly smaller than that of NF insert_th after 14 days, resulting in a lower maximum TEER value compared to that of NF insert_th (Fig. b (ii)–(iii)). Given that the culture conditions provided to the cells were exactly the same, whereas the bonding methods were different, we assumed that the difference in the TEER values might have occurred because of leakage at the

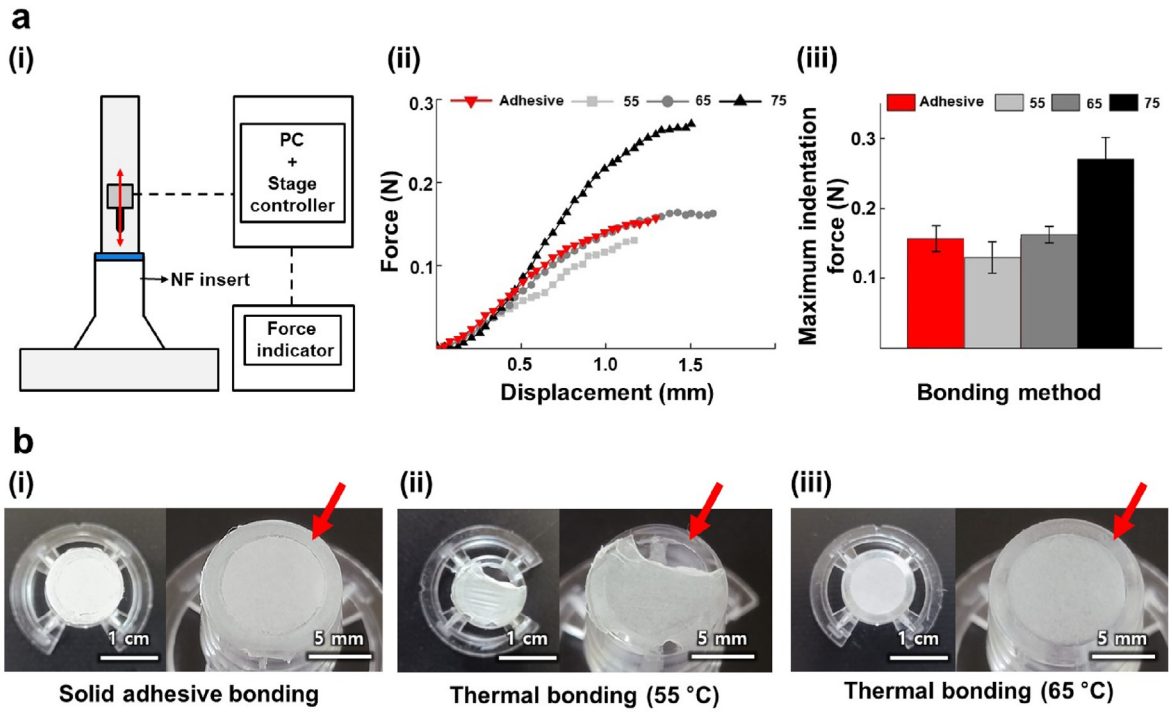

Fig. 3. (a) Indentation test setup and results: (i) schematic of the indentation test setup; (ii) measured indentation force of NF membrane bonded by solid adhesive and localized thermal bonding depending on T_{PS}. (iii) Maximum indentation force of NF membrane for different bonding methods. (b) Images of NF membrane after soaking in culture media for 3 days for different bonding methods: (i) NF insert_ad, (ii) NF insert_th bonded at 55 °C, and (iii) NF insert_th bonded at 65 °C.

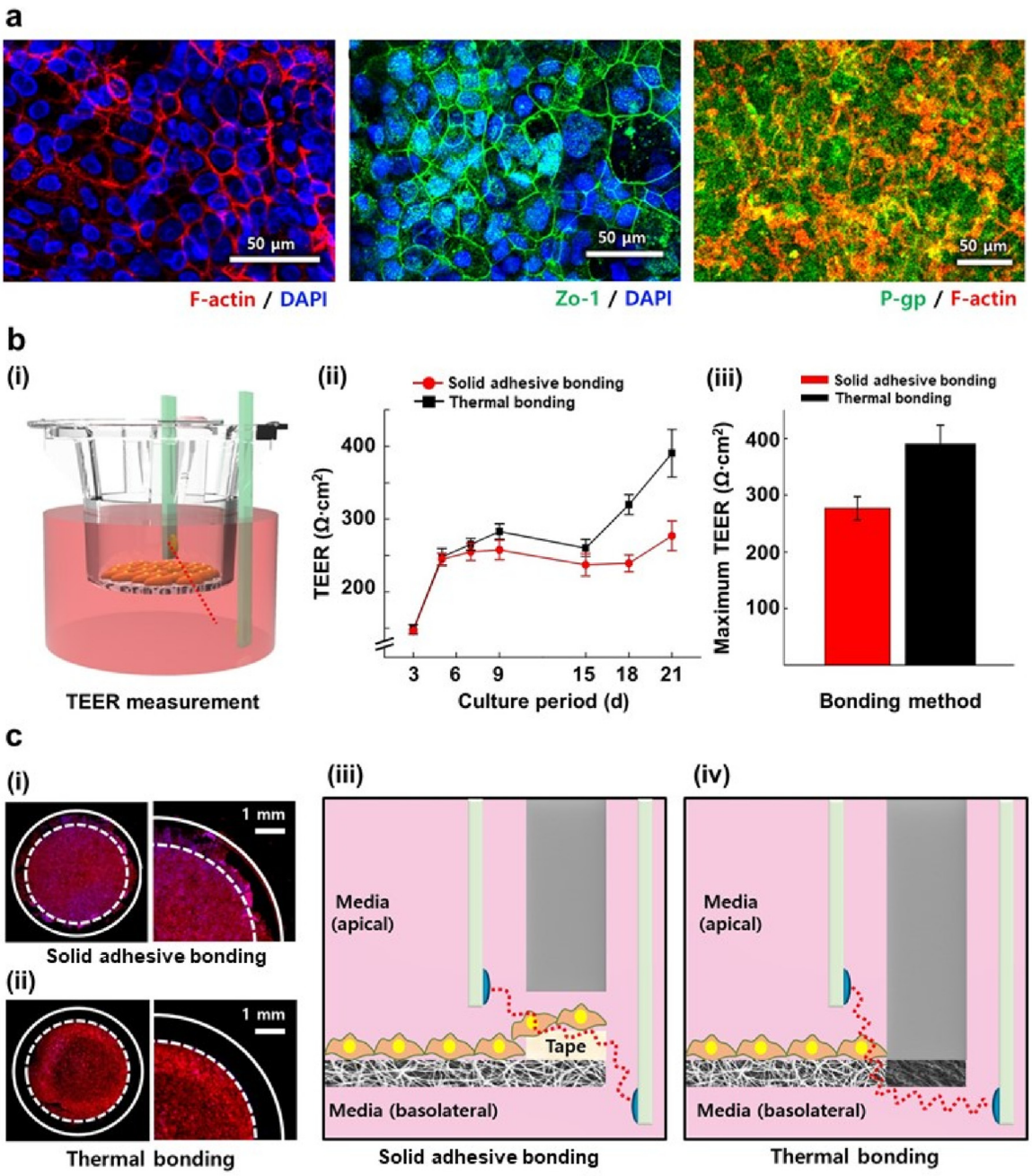

Fig. 4. (a) Immunofluorescence images of Caco-2 cells cultured on NF insert_th. (b) TEER measurement of NF insert_th and NF insert_ad: (i) schematic image of TEER measurement; (ii) TEER value measured for 21 days, and (iii) maximum TEER value of each bonding method during cell culture. (n = 5) (c) Caco-2 cells immunostained with phalloidin (red) and DAPI (blue) near the bonding interface of (i) NF insert_ad and (ii) NF insert_th. Schematic illustration explaining TEER value difference between (iii) NF insert_ad and (iv) NF insert_th. (For interpretation of the references to color in this figure legend, the reader is referred to the Web version of this article.)

TP–NF bonding interface formed by the solid adhesive of NF insert_ad (Fig. 4c).

3.5. *Practical application of thermal bonding to fabrication of NF culture platforms*

Beyond NF inserts, the thermal bonding method is applicable to the fabrication of various types of culture platforms with different purposes and geometries. The NF membrane could be integrated into a TP grid or microfluidic channel using the thermal bonding method to fabricate NF membrane-integrated culture chambers and microfluidic chips (Fig. 5a and b). The NF membrane could also be imprinted on TP substrates in several patterns using heated stamps, as shown in Fig. 5c. Furthermore, a 3D NF membrane could be integrated onto the TP substrate and then be used to fabricate a 3D microwell-shaped NF membrane-integrated culture insert (NF microwell insert) for cell spheroid culture, which was developed in our previous study [16] (Fig. 5d).

We further demonstrated the wide applicability of thermally bonded NF culture platforms by developing dynamic-cultured, cocultured, or 3D spheroid-cultured *in vitro* organ models: 1) a microfluidic skin-on-a-chip model composed of keratinocytes, fibroblasts, type I collagen hydrogel, and fluid flow on an NF microfluidic chip; 2) BBB coculture model with iPSC-derived brain endothelial cells and astrocytes on an NF insert; 3) 3D iPSC spheroid model on an NF microwell insert (Fig. 6).

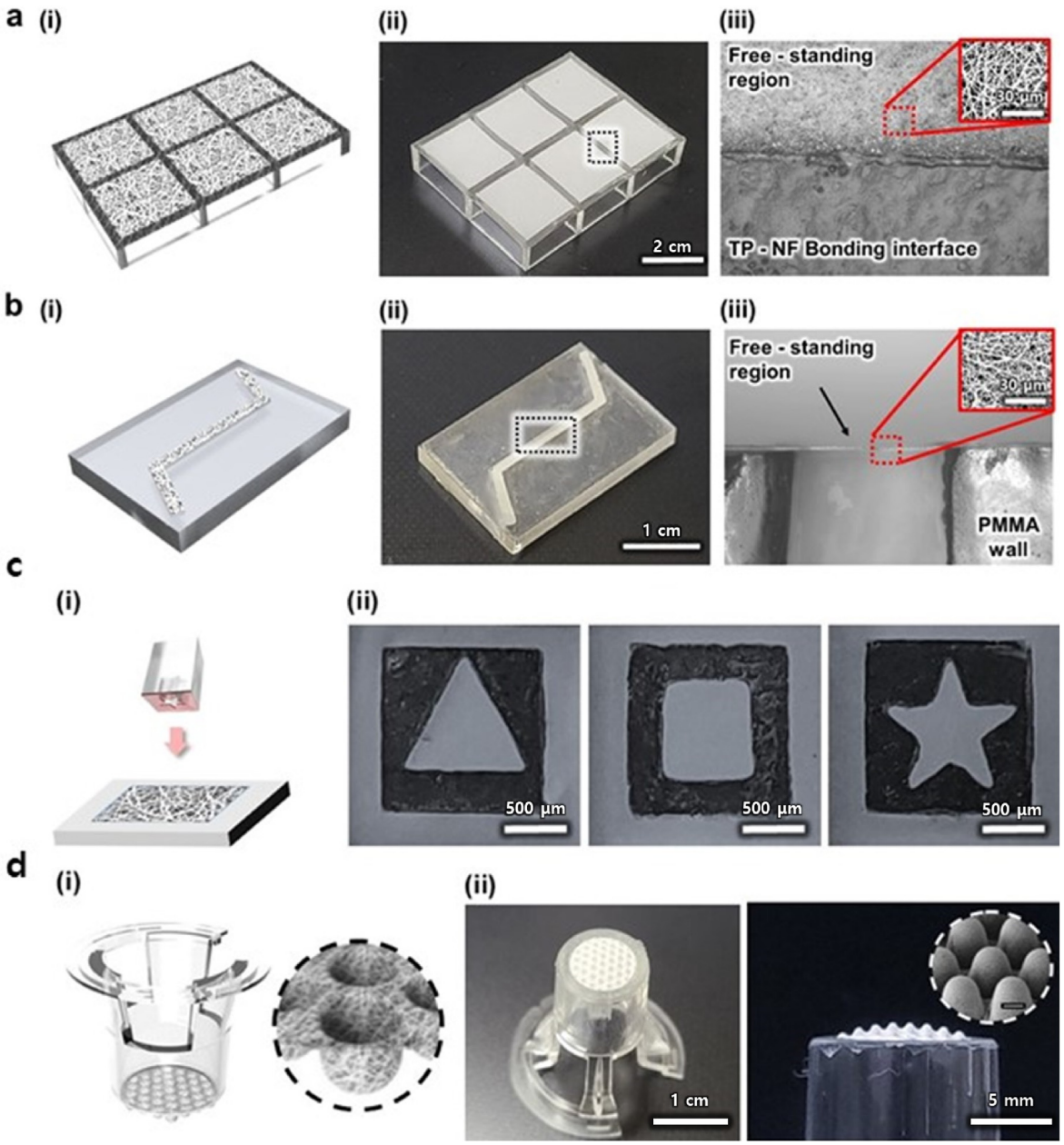

Fig. 5. Versatile application of localized thermal bonding process on fabrication of *in vitro* cell culture platforms. (a) Nanofiber membrane bonded on the grid: (i) schematic illustration of NF-integrated culture chamber, (ii) camera image of fabricated NF-integrated culture chamber, and (iii) microscopic image of NF membrane near the TP–NF bonding interface. (b) NF membrane bonded on a microfluidic chip: (i) schematic illustration of NF-integrated microfluidic chip, (ii) camera image of fabricated NF-integrated PMMA microfluidic chip, and (iii) microscopic image of NF membrane near channel and free-standing region. (c) NF bonding on surface by stamping: (i) schematic illustration of NF membrane bonding by stamping and bonded NF membrane on PS surface in shapes of (ii) triangle, (iii) square, and (iv) star. (d) 3D microwell-shaped nanofiber membrane bonded on a culture insert: (i) schematic illustration of 3D NF microwell-integrated culture insert and its (ii) camera image and (iii) microscopic and SEM images.

4. Discussion

Recently, NF membranes have emerged as versatile and functional materials possessing high surface-to-volume ratios, high permeabilities, and ECM-like biomimetic architectures derived from their unique nanofibrous structures. However, these nanofibrous structures also make it difficult for NF membranes to stably bond onto disposable TP supporting substrates, which is very significant to the practical utilization of NF membranes. Although solid adhesives and complex external clamping devices have been utilized to bond NF membranes onto TP substrates, the potential negative effects of adhesives on cells or the complicated bonding processes further hinder the utilization of NF membranes in biomedical applications.

Herein, we propose a facile but suitable method for bonding an NF membrane onto a TP supporting substrate based on localized thermal heating. The main challenge in applying the proposed localized thermal bonding method to NF membranes involves preventing structural damage to nanofibers in the free-standing region induced by excessive heat transfer. Therefore, we have developed a numerical heat transfer simulation model to determine the proper preheating temperature for the TP supporting substrate such that sufficient heat is provided for the NFs to be melted at the TP–NF bonding interface while preventing overheating that

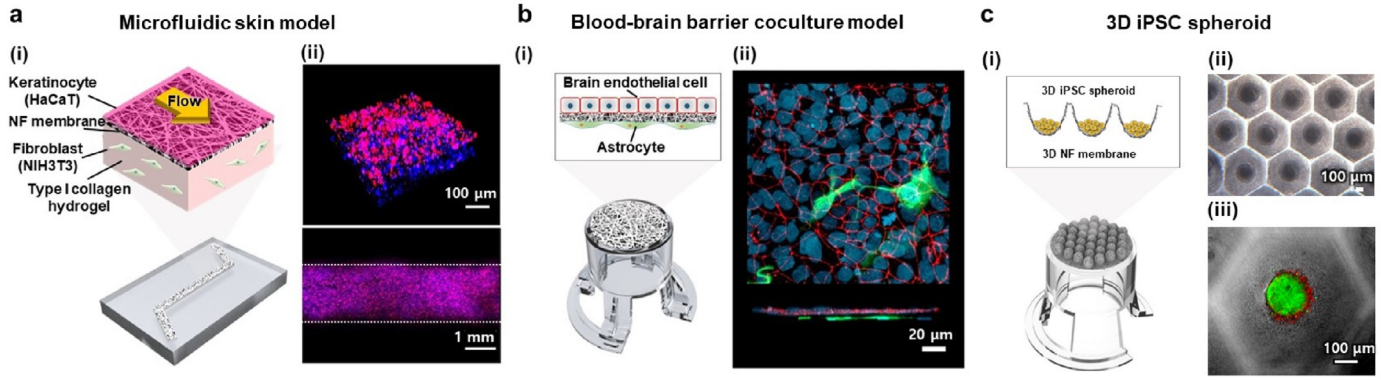

Fig. 6. *In vitro* models constructed on various types of NF membrane-integrated culture platforms. (a) Microfluidic skin model constructed on NF microfluidic chip and its (i) schematic illustration and (ii) confocal microscopic images showing 3D view and top view of the channel. HaCaT cells stained with both phalloidin (magenta) and DAPI (blue) and NIH3T3 cells in type I collagen hydrogel layer stained with only DAPI (blue). (b) Blood–brain barrier coculture model constructed on NF insert and its (i) schematic illustration and (ii) confocal microscopic images showing top view and cross-section view. iPSC-derived brain microvascular endothelial cells stained with both ZO-1 (red) and DAPI (blue) and astrocytes stained with GFAP (green). (c) 3D iPSC spheroid model constructed on NF microwell insert and its (i) schematic illustration, (ii) microscopic image, and (iii) confocal microscopic image of iPSC cells stained with calcein AM (green) and propidium iodide (red). (For interpretation of the references to color in this figure legend, the reader is referred to the Web version of this article.)

can induce the melting of NFs in the free-standing region. The simulation model successfully predicted spatiotemporal temperature changes in and near the PS culture insert, allowing us to estimate the region where the NFs would be melted. Based on the simulation results, we could find the optimal T_{PS} for the proper bonding of the PCL NF membrane onto the PS culture insert. The optimal T_{PS} was found to be slightly above $T_{m\text{-}PCL}$ (approximately 5 °C above), which was sufficient to melt the NFs only at the TP–NF bonding interface. When the PS culture insert was preheated excessively above $T_{m\text{-}PCL}$, it resulted in the melting of the NFs not only at the TP–NF bonding interface but also in the free-standing region.

Based on the optimized preheating temperature, the PCL NF membrane can be bonded onto the PS culture insert after a simple transfer process that does not require additional pressure. The NFs are melted to form a bonding interface within 2 s after the transfer. We evaluated the bonding strength of the PCL NF membrane, which was bonded onto the PS culture insert using the proposed bonding method, not only using an indentation testing machine but also by examining the inserts under wet conditions. The results of the bonding stability evaluation demonstrated that the proposed thermal bonding method for NF membranes ensured a bonding strength comparable to that of solid adhesive bonding with a similar maximum indentation force. Furthermore, the thermally bonded interface was stable even under wet conditions.

The bonding stability of NF insert_th under cell culture conditions was demonstrated using a long-term culture of human intestinal Caco-2 epithelial cells. The TP–NF bonding interface formed at the optimal T_{PS} successfully supported the culturing of Caco-2 cells on the PCL NF membrane until the cells fully differentiated to express the key proteins of ZO-1 and P-gp. Interestingly, the TEER value was remarkably higher for NF insert_th than for NF insert_ad as the culture time passed. Because all culture conditions for the two groups were the same, whereas the bonding methods were different, we assumed that the bonding method might have affected the TEER value. To confirm whether there was leakage at the TP–NF bonding interface of each NF insert, we stained the Caco-2 cells in both NF insert_ad and NF insert_th. As shown in Fig. 4c (i)–(ii), there were some cells on the TP–NF bonding interface of NF insert_ad, whereas no cells were found at the TP–NF bonding interface of NF insert_th. These results imply that there are undesired gaps at the TP–NF bonding interface of NF insert_ad, allowing the infiltration of cells between the NF membrane and PS substrate during the long culture period. Furthermore, we directly observed several buckled NF membrane regions for NF insert_ad induced by delamination from the PS wall, as shown in Fig. S4. It could be inferred that the long-term exposure of the TP–NF bonding interface to wet culture conditions might have loosened the bonding of the solid adhesive, resulting in local delamination of the NF membrane. These results are consistent with the measured lower TEER value in the case of NF insert_ad, which may have been caused by gaps between the NF membrane and PS culture insert, as depicted in Fig. 4c (iii)–(iv). The cell culture results show that the proposed localized thermal bonding method demonstrates superior stability compared to that of conventional solid adhesive bonding under wet cell culture conditions over a long period of time. These results indicate that the localized thermal bonding method is not only facile but also sufficiently functional to be utilized in the fabrication of an NF-based *in vitro* culture platform.

Although we demonstrate the applicability of the localized thermal bonding method only to the bonding of a PCL NF membrane onto a PS culture insert, the proposed localized thermal bonding method is versatile in terms of not only geometry (Fig. 5) but also TP material, including polymethylmethacrylate, which is also a well-known material for cell culture platforms (Fig. S5). Furthermore, although we have applied the thermal bonding method only to NF membranes with a thickness of 30 μm a representative case, the bonding method is inferred to be potentially applicable to NF membranes having various thicknesses. The thermal bonding method can also be applied to other types of NF materials. For example, the PCL-F NF membrane, which was made up of a PCL solution mixed with Pluronic F-108 for enhanced hydrophilicity, can be bonded onto PS and PMMA substrates using the thermal bonding method (Fig. S5). However, T_m of the NF should be lower than T_g (glass transition temperature) of the TP to prevent the deformation of the heated TP culture substrate. Based on the T_g values of typical thermoplastics for cell culture platforms, which is approximately 100 °C, the thermal bonding method is applicable to NF membranes with T_m below 100 °C. The proposed bonding method could be used to integrate 2D or 3D NF membranes on TP supporting substrates with wide areas, multiple regions, or complex or precise structures, such as microfluidic channels. Furthermore, the NF membrane could be readily imprinted on a TP supporting substrate with a desired pattern via a simple stamping process based on localized heating. This localized thermal bonding method suggests a new method for fabricating NF membrane-integrated platforms without the addition of any external materials for bonding, thereby demonstrating the ease, robustness, and versatility of the bonding method. The proposed thermal bonding method can realize the potential of NF membranes for the development of advanced and biomimetic organs-on-a-chip, high-throughput cell culture platforms, coculture platforms, and 3D spheroid culture platforms.

5. Conclusion

This study proposes a facile, leakage-free, and structural damage-free method for bonding NF membranes onto supporting substrates via localized heating. Optimal preheating conditions were determined efficiently using a newly developed numerical heat transfer model. The bonding stability of the TP–NF bonding interface formed via the localized thermal bonding method was found to be comparable to that of conventional solid adhesive bonding, but even more stable and long-lasting under wet culture conditions. The localized thermal bonding method was determined to be applicable to various NF and TP materials, including PCL and PS, with various geometries ranging from a culture insert to a microfluidic chip, which are representative materials and structures, respectively, for *in vitro* culture platforms. Therefore, the proposed localized thermal bonding method can broaden and realize various practical applications for functional NF membranes in the biomedical field.

Credit author statement

Conceptualization: J.Y. and D.S.K, Methodology: J.Y. and J.R.Validation: J.R, Formal analysis: J.R.Investigation: J.Y. and J.R.Resources: J.Y., J.R., D.K., J.L.,and J-W.C.Writing-Original Draft: J.Y. and J.R.Writing-Review & Editing: J.Y. and D.S.K.Supervision: D.S.K. and T-E.P.Funding acquisition: D.S.K. and T-E.P.

Declaration of competing interest

The authors declare that they have no known competing financial interests or personal relationships that could have appeared to influence the work reported in this paper.

Data availability

Data will be made available on request.

Acknowledgements

This work was supported by the National Research Foundation of Korea (NRF) grant funded by the Korea government (MSIT) (No.RS-2023-00208702 to D.S.K. and 2020R1C1C1014753 to T-E.P.).

Appendix A. Supplementary data

Supplementary data to this article can be found online at https://doi.org/10.1016/j.mtbio.2023.100648.

References

[1] S. Wu, T. Dong, Y. Li, M. Sun, Y. Qi, J. Liu, M.A. Kuss, S. Chen, B. Duan, State-of-the-art review of advanced electrospun nanofiber yarn-based textiles for biomedical applications, Appl. Mater. Today 27 (2022), 101473, https://doi.org/10.1016/j.apmt.2022.101473.

[2] Y. Qi, C.E. Wang, Q.Y. Wang, F. Zhou, T. Li, B. Wang, W.D. Su, D.W. Shang, S.H. Wu, A simple, quick, and cost-effective strategy to fabricate polycaprolactone/silk fibroin nanofiber yarns for biotextile-based tissue scaffold application, Eur. Polym. J. 186 (2023), https://doi.org/10.1016/j.eurpolymj.2023.111863.

[3] Y.J. Chen, X.T. Dong, M. Shafiq, G. Myles, N. Radacsi, X.M. Mo, Recent advancements on three-dimensional electrospun nanofiber scaffolds for tissue engineering, Adv Fiber Mater 4 (5) (2022) 959–986, https://doi.org/10.1007/s42765-022-00170-7.

[4] X.L. Zhang, Q.L. Qu, A.Q. Yang, J. Wang, W.X. Cheng, Y.K. Deng, A.Y. Zhou, T. Lu, R.H. Xiong, C.B. Huang, Chitosan enhanced the stability and antibiofilm activity of self-propelled Prussian blue micromotor, Carbohydr. Polym. 299 (2023), https://doi.org/10.1016/j.carbpol.2022.120134.

[5] Y.K. Deng, T. Lu, J.X. Cui, S.K. Samal, R.H. Xiong, C.B. Huang, Bio-based electrospun nanofiber as building blocks for a novel eco-friendly air filtration membrane: a review, Sep. Purif. Technol. 277 (2021), https://doi.org/10.1016/j.seppur.2021.119623.

[6] R. Gao, Y. Jing, Y. Ni, Q. Jiang, Effects of chitin nanocrystals on coverage of coating layers and water retention of coating color, J. Bioresour. Bioprod. 7 (3) (2022) 201–210, https://doi.org/10.1016/j.jobab.2021.11.003.

[7] J. Xiao, H. Li, H. Zhang, S. He, Q. Zhang, K. Liu, S. Jiang, G. Duan, K. Zhang, Nanocellulose and its derived composite electrodes toward supercapacitors: fabrication, properties, and challenges, Journal of Bioresources and Bioproducts 7 (4) (2022) 245–269, https://doi.org/10.1016/j.jobab.2022.05.003.

[8] T. Lu, H.B. Liang, W.X. Cao, Y.K. Deng, Q.L. Qu, W.J. Ma, R.H. Xiong, C.B. Huang, Blow-spun nanofibrous composite Self-cleaning membrane for enhanced purification of oily wastewater, J. Colloid Interface Sci. 608 (2022) 2860–2869, https://doi.org/10.1016/j.jcis.2021.11.017.

[9] T. Lu, W.X. Cao, H.B. Liang, Y.K. Deng, Y.Y. Zhang, M.M. Zhu, W.J. Ma, R.H. Xiong, C.B. Huang, Blow-Spun nanofibrous membrane for simultaneous treatment of emulsified oil/water mixtures, dyes, and bacteria, Langmuir 38 (50) (2022) 15729–15739, https://doi.org/10.1021/acs.langmuir.2c02620.

[10] S.H. Jiang, H. Schmalz, S. Agarwal, A. Greiner, Electrospinning of ABS nanofibers and their high filtration performance, Adv Fiber Mater 2 (1) (2020) 34–43, https://doi.org/10.1007/s42765-019-00026-7.

[11] J. Youn, H. Hong, W. Shin, D. Kim, H.J. Kim, D.S. Kim, Thin and stretchable extracellular matrix (ECM) membrane reinforced by nanofiber scaffolds for developing in vitro barrier models, Biofabrication 14 (2) (2022), https://doi.org/10.1088/1758-5090/ac4dd7.

[12] J. Youn, H. Han, S.M. Park, D.S. Kim, Arterial internal elastic lamina-inspired membrane for providing biochemical and structural cues in developing artery-on-a-chip, ACS Macro Lett. 10 (11) (2021) 1398–1403, https://doi.org/10.1021/acsmacrolett.1c00551.

[13] X.Y. Yang, K.Y. Li, X. Zhang, C. Liu, B.K. Guo, W.J. Wen, X.H. Gao, Nanofiber membrane supported lung-on-a-chip microdevice for anti-cancer drug testing, Lab Chip 18 (3) (2018) 486–495, https://doi.org/10.1039/C7LC01224A.

[14] S.C. Slater, V. Beachley, T. Hayes, D.M. Zhang, G.I. Welsh, M.A. Saleem, P.W. Mathieson, X.J. Wen, B. Su, S.C. Satchell, An in vitro model of the glomerular capillary wall using electrospun collagen nanofibres in a bioartificial composite basement membrane, PLoS One 6 (6) (2011), https://doi.org/10.1371/journal.pone.0020802.g010.

[15] G. Salimbeigi, N.E. Vrana, A.M. Ghaemmaghami, P.Y. Huri, G.B. McGuinness, Basement membrane properties and their recapitulation in organ-on-chip applications, Mater Today Bio 15 (2022), https://doi.org/10.1016/j.mtbio.2022.100301.

[16] D. Kim, S.J. Lee, J. Youn, H. Hong, S. Eom, D.S. Kim, A deep and permeable nanofibrous oval-shaped microwell array for the stable formation of viable and functional spheroids, Biofabrication 13 (3) (2021), https://doi.org/10.1088/1758-5090/ac044c.

[17] E. Rofaani, J. Peng, L. Wang, Y. He, B.X. Huang, Y. Chen, Fabrication of ultrathin artificial basement membrane for epithelial cell culture, Microelectron. Eng. 232 (2020), https://doi.org/10.1016/j.mee.2020.111407.

[18] J.W. Choi, J. Youn, D.S. Kim, T.E. Park, Human iPS-derived blood-brain barrier model exhibiting enhanced barrier properties empowered by engineered basement membrane, Biomaterials 293 (2023), 121983, https://doi.org/10.1016/j.biomaterials.2022.121983.

[19] J. Rhyou, J. Youn, S. Eom, D.S. Kim, Facile fabrication of electrospun nanofiber membrane-integrated PDMS microfluidic chip via silver nanowires-uncured PDMS adhesive layer, ACS Macro Lett. 10 (7) (2021) 965–970, https://doi.org/10.1021/acsmacrolett.1c00256.

[20] Y.H. Guo, Y.C. Guo, W.D. He, Y.B. Zhao, R.Q. Shen, J.X. Liu, J. Wang, PET/TPU nanofiber composite filters with high interfacial adhesion strength based on one-step co-electrospinning, Powder Technol. 387 (2021) 136–145, https://doi.org/10.1016/j.powtec.2021.04.020.

[21] B. Zhang, X. Yan, Y. Xu, H.S. Zhao, M. Yu, Y.Z. Long, Measurement of adhesion of in situ electrospun nanofibers on different substrates by a direct pulling method, Adv. Mater. Sci. Eng. 2020 (2020), https://doi.org/10.1155/2020/7517109.

[22] S. Smith, M. Delaney, M. Frey, Anti-Escherichia coli functionalized silver-doped carbon nanofibers for capture of E. coli in microfluidic systems, Polymers 12 (5) (2020), https://doi.org/10.3390/polym12051117.

[23] L.E. Stallcop, Y.R. Alvarez-Garcia, A.M. Reyes-Ramos, K.P. Ramos-Cruz, M.M. Morgan, Y.T. Shi, L.J. Li, D.J. Beebe, M. Domenech, J.W. Warrick, Razor-printed sticker microdevices for cell-based applications, Lab Chip 18 (3) (2018) 451–462, https://doi.org/10.1039/C7LC00724H.

[24] D. Kim, S. Eom, S.M. Park, H. Hong, D.S. Kim, A collagen gel-coated, aligned nanofiber membrane for enhanced endothelial barrier function, Sci Rep-Uk 9 (2019), https://doi.org/10.1038/s41598-019-51560-8.

[25] M. Radiom, Y. He, J. Peng-Wang, A. Baeza-Squiban, J.F. Berret, Y. Chen, Alveolar mimics with periodic strain and its effect on the cell layer formation, Biotechnol. Bioeng. 117 (9) (2020) 2827–2841, https://doi.org/10.1002/bit.27458.

[26] J.H. Kim, J.Y. Park, S. Jin, S. Yoon, J.Y. Kwak, Y.H. Jeong, A microfluidic chip embracing a nanofiber scaffold for 3D cell culture and real-time monitoring, Nanomater.-Basel 9 (4) (2019), https://doi.org/10.3390/nano9040588.

[27] K.H. Lee, D.J. Kim, B.G. Min, S.H. Lee, Polymeric nanofiber web-based artificial renal microfluidic chip, Biomed. Microdevices 9 (4) (2007) 435–442, https://doi.org/10.1007/s10544-007-9047-5.

[28] S.M. Park, H. Kim, K.H. Song, S. Eom, H. Park, J. Doh, D.S. Kim, Ultra-thin, aligned, free-standing nanofiber membranes to recapitulate multi-layered blood vessel/tissue interface for leukocyte infiltration study, Biomaterials 169 (2018) 22–34, https://doi.org/10.1016/j.biomaterials.2018.03.053.

[29] J. Ma, Q. Zhang, Y. Zhang, L. Zhou, J.K. Yang, Z.H. Ni, A rapid and simple method to draw polyethylene nanofibers with enhanced thermal conductivity, Appl. Phys. Lett. 109 (3) (2016), https://doi.org/10.1063/1.4958905.

[30] J. Ma, Q. Zhang, A. Mayo, Z. Ni, H. Yi, Y. Chen, R. Mu, L.M. Bellan, D. Li, Thermal conductivity of electrospun polyethylene nanofibers, Nanoscale 7 (40) (2015) 16899–16908, https://doi.org/10.1039/C5NR04995D.
[31] J.J. Xue, M. He, Y.Z. Niu, H. Liu, A. Crawford, P. Coates, D.F. Chen, R. Shi, L.Q. Zhang, Preparation and in vivo efficient anti-infection property of GTR/GBR implant made by metronidazole loaded electrospun polycaprolactone nanofiber membrane, Int. J. Pharm. 475 (1–2) (2014) 566–577, https://doi.org/10.1016/j.ijpharm.2014.09.026.
[32] H.B. Chong, J. Youn, W. Shin, H.J. Kim, D.S. Kim, Multiplex recreation of human intestinal morphogenesis on a multi-well insert platform by basolateral convective flow, Lab Chip 21 (17) (2021) 3316–3327, https://doi.org/10.1039/D1LC00404B.